

# Optical design and fabrication of zinc selenide microlens array with extended depth of focus for biomedical imaging

**Article history:**

Received: 21-10-2022

Revised: 5-01-2023

Accepted: 20-01-2023

Neha Khatri<sup>a</sup>, Sonam Berwal<sup>b</sup>, K. Manjunath<sup>c</sup>, Bharpoor Singh<sup>d</sup>

**Abstract:** Optical coherence tomography is a well-known technique for the optical imaging of biological tissues. However, the depth scanning range of high-resolution optical coherence tomography is restricted by its depth of focus. In this study, a Zinc Selenide (ZnSe) Microlens Array (MLA) is employed to overcome the depth-of-focus limitation of optical coherence tomography. The ZnSe material with a low Abbe number and high chromatic dispersion extends the depth of focus with transverse resolution. The ZnSe MLA focused the incident light (from visible to near-infrared (NIR) region) on multiple focal planes with the uniform distribution of light over a biological tissue. The MLA is designed using Zemax OpticStudio software and fabricated via a single-point diamond-turning based on Slow Tool Servo (STS) configuration. STS machining has the unique advantage of offering larger degrees of freedom with no additional baggage, thereby reducing the setup time. The experimental results show the effectiveness of the STS machining process in fabricating ZnSe MLA with desired accuracies. The characterization of fabricated MLA using Coherence Correlation Interferometry (CCI) depicts uniform lenslets with no structural and positional distortion, with a total error of 32 nm within the tolerance limit.

**Keywords:** optical coherence tomography; microlens array; zinc selenide; slow tool servo; optical design.

<sup>a</sup> CSIR-Central Scientific Instruments Organisation, Chandigarh 160030, India. Academy of Scientific & Innovative Research (AcSIR), Ghaziabad 201002, India. Corresponding author: nehakhatri@csio.res.in

<sup>b</sup> CSIR-Central Scientific Instruments Organisation, Chandigarh 160030, India. Academy of Scientific & Innovative Research (AcSIR), Ghaziabad 201002, India.

<sup>c</sup> CSIR-Central Scientific Instruments Organisation, Chandigarh 160030, India. Academy of Scientific & Innovative Research (AcSIR), Ghaziabad 201002, India.

<sup>d</sup> CSIR-Central Scientific Instruments Organisation, Chandigarh 160030, India.

© The Author(s), 2023

## 1. INTRODUCTION

Optical coherence tomography (OCT) is a non-invasive high-resolution optical imaging technology predominantly utilized for 3-D imaging biomedical tissues. The working of OCT is based on the interference phenomenon between a local reference signal and a signal from an object under investigation (Podoleanu, 2012). OCT is used in the biomedical domain for numerous applications (Romodina *et al.*, 2022), including ophthalmology (Sakata *et al.*, 2009; Singh *et al.*, 2011), cardiology (Giattina *et al.*, 2006), and endoscopy of the gastrointestinal tract (Dong *et al.*, 2022; Tsai *et al.*, 2017). OCT also enables high resolution up to micrometre level along with a few mm penetration depths (Singh *et al.*, 2018). The axial resolution is defined as the resolution along light beam propagation, which is inversely proportional to the width of the light source spectrum. Thus, the axial resolution can be improved by using a broadband light source. However, the lateral resolution depends on the imaging lens numerical aperture (NA). The lateral resolution is significantly reduced when the focal point of the imaging lens moves away from the focus spot of light due to the rapid

divergence (Romodina *et al.*, 2022). A beam cannot be produced from a spherical lens with an extended focal depth and a narrow lateral width (Ding *et al.*, 2002). Hence, the lateral resolution and the depth of focus (DOF) with traditional optics in OCT significantly limit the range of applications. Additionally, dynamic focusing lenses are bulky and need more space during the system assembly.

In recent years, the scientific community have shown a tremendous evolution to overcome the DOF limitation in OCT for high lateral resolution. In 2002, Ding *et al.* proposed a study based on an axicon lens (Ding *et al.*, 2002). The authors declared that an axicon lens could be used in an OCT system to maintain high lateral resolution over a greater depth of field, which is essential for high-resolution, high-speed OCT. However, the imaged part carried only ~5% of the total power, which limits its application for biomedical samples. In 2007, Liu *et al.* reported the axial and lateral behaviours of four-zone binary-phase spatial filters to extend the DOF (Liu *et al.*, 2007). However, in the proposed approach, the beam has a Bessel intensity distribution than the Gaussian, which suffers from the significant loss of spatial frequency components in the coherence transfer function. Due to this, sensitivity reduces, and sidelobe artefacts are seen in the OCT images. Ortega and the group proposed a study on wide-field OCT using microlens arrays. The authors primarily focused on DOF and scanning speed. Initially, MLA are used to accelerate scanning speed over the object surface (Ortega *et al.*, 2007). After that, to increase the DOF, a lengthening compensating path is introduced in the interferometer arm (Ortega *et al.*, 2007). In 2017, Bo *et al.* presented a novel method to overcome the DOF limitation in OCT through multiple aperture synthesis without sidelobe artefacts (Bo *et al.*, 2017).

Nevertheless, this technique requires transversal shifting of a micro cylindrical lens near the tip of the sample fiber during the imaging process, which is responsible for limiting the speed of imaging (Bo *et al.*, 2017). Few researchers also utilized adaptive optics to extend DOF by dynamic control of deformable mirrors (Sasaki *et al.*, 2012). Recently, Romodina *et al.* (Romodina *et al.*, 2022) extended the DOF by employing ultrahigh chromatic dispersion of ZnSe. ZnSe material has a strong spectral dispersion in the visible and NIR regions. However, the single ZnSe lens focused the incident light on multiple focal planes with the nonuniform light distribution.

In this research article, a ZnSe MLA is designed and fabricated to homogenize the incident light over a biological tissue or sample. In OCT imaging, ZnSe MLA with a low Abbe number and high chromatic dispersion extends the DOF with transverse resolution. The novelty of the proposed ZnSe MLA study is to split the source beam into a grid of beamlets to obtain uniform light distribution over the biological tissue, reducing the scanning time and improving the scanning speed. An (11 × 11) plano-convex MLA is designed using the Zemax OpticStudio and fabricated by using single-point diamond turning (SPDT, Nanoform-200) with slow tool servo (STS) configuration. The manufacturing of the ZnSe MLA using the STS optimum tool path with no additional setup is another aspect of this study. After fabrication, the MLA is characterized using a coherence correlation interferometer (CCI) with a 5X objective.

## 2. OPTICAL DESIGN

The design of any optical element is advantageous in reducing effort and time consumption while fabricating and assembling various components. The rectangular (11 × 11) plano-convex MLA is designed using the Zemax OpticStudio. The design of plano-convex microlens is based on the lens diameter ( $\Phi$ ), height at the vertex (hL), radius of curvature (R), and refractive index (n). Numerous iterations have been performed to optimize the lenslet's radius of curvature and focal length. The MLA is optimized using the multiparameter optimization method for uniform incident light illumination. The multiparameter optimization method is an indirect method in which the initial microlens surface is first established. Afterwards, the design parameters are optimized until the desired outcome is achieved. The designed ZnSe array of microlens split the beam into a grid of beamlets, as illustrated in Fig. 1.

The lens profile  $h(r)$  of an axial symmetrical plano-convex lens is determined by equation 1 (Berwal *et al.*, 2022).

$$h(r) = \frac{1}{R} \frac{r^2}{1 + \sqrt{1 - (1+k)\left(\frac{r^2}{R^2}\right)}} + \sum_{n=2}^m A_{2n} r^{2n} \quad (1)$$

where  $h$  is the height of the lens as a function of the distance ( $r$ ) to the optical axis. The lens profile  $h(r)$  for a spherical (plano-convex) lens is ( $K = 0$ ).

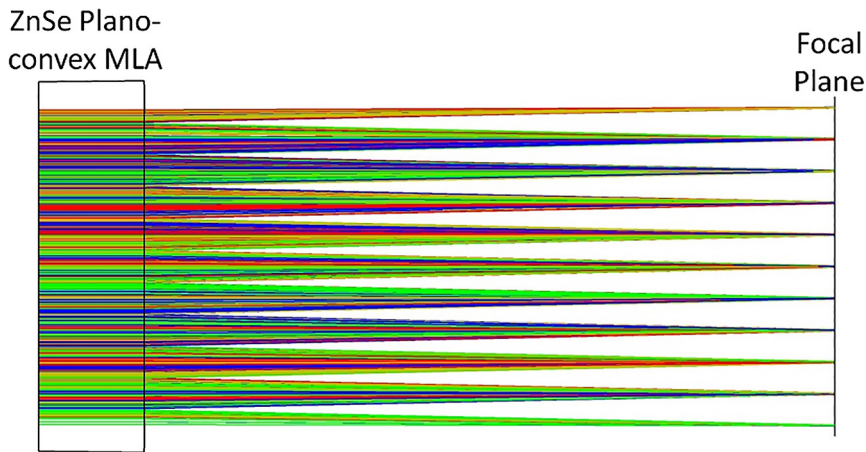


**Figure 1.** Splitting of incident light into a grid of beamlets via (11 × 11) plano-convex MLA.

Fig. 2 shows the rectangular MLA with surface geometry parameters (pitch (P), radius (R), and height (h<sub>L</sub>)) of the single microlens. The radius of curvature (R) at the vertex is calculated by equation 2 (Nussbaum *et al.*, 1997).

$$R = (K+1) \frac{h_L}{2} + \frac{r^2}{2h_L} \tag{2}$$

where h<sub>L</sub> is the height at the vertex.

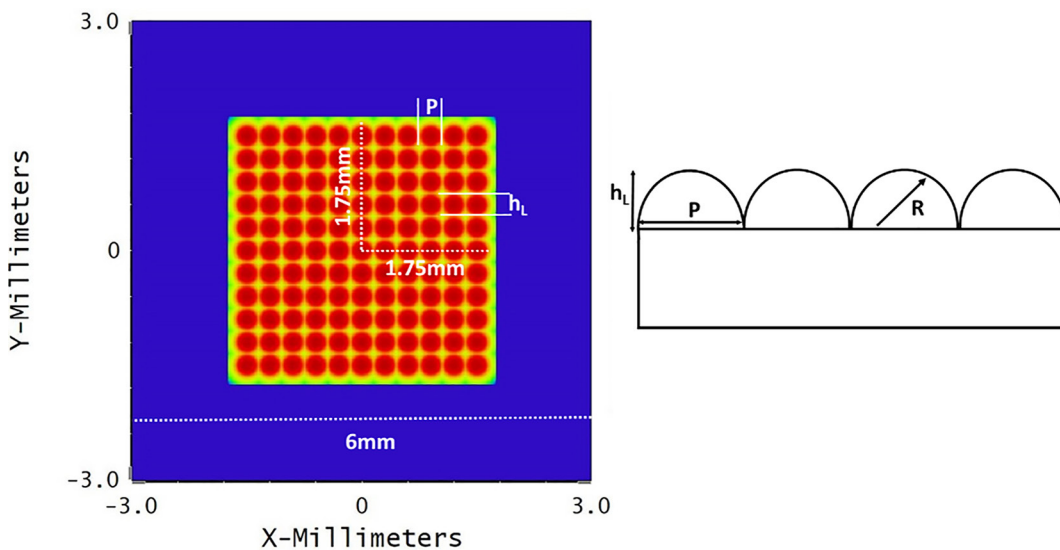


**Figure 2.** Rectangular MLA with surface geometry design.

All microlens in the array has an identical focal length to collimate the beamlets. The focal length (f) of a plano-convex refractive lens is calculated by equation 3 (Nussbaum *et al.*, 1997).

$$f = \frac{R}{n(\lambda)-1} \tag{3}$$

Table 1 shows the detailed data for the design of (11 × 11) ZnSe plano-convex MLA. The ZnSe material is quite popular as a striking infrared crystal and used for night vision systems. However, due to high brittleness, low hardness, and polycrystalline structure formed by the randomly oriented grains causes different forms of micro-cracks (or) pits remain on the final machined surface making the

fabrication challenging (Geng *et al.*, 2021; Xiao *et al.*, 2019). Accordingly, the microlens array's fabrication is considered in the present research.

Substrate Material	Zinc Selenide (ZnSe)
Wavelength Range ( $\lambda$ )	Visible to NIR
Array Type	Rectangular, 11 × 11
Lens Type	Plano-convex
Lenslet Pitch	0.3 mm
Lenslet Radius	9.9 mm
Lenslet Height	0.3 mm
Focal Length	6.497 mm
AR Coating	No

**Table 1.** Design parameters of the microlens array.

### 3. FABRICATION OF ZnSE MLA

A wide variety of machining methods are used to fabricate MLA; among them, diamond turning is superior due to high efficiency and repeatability for applications in optics, aerospace and biomedical. Methods like photolithography (Lim *et al.*, 2006b), laser patterning (Lim *et al.*, 2006a) and focus ion beam (Lee *et al.*, 2007), and Embossing (Moore *et al.*, 2016) are also reported in the literature. Still, all these methods have the disadvantage of poor uniformity in terms of surface accuracy, limitations of geometric size, and low efficiency (Yuan *et al.*, 2018). Three diamond turning processes are pretty famous for the fabrication of MLA: Slow Tool Servo (STS), Fast Tool Servo (FTS), Broaching and Diamond Milling (DM) (Klocke *et al.*, 2013; Yin *et al.*, 2011). DM requires an additional milling axis and the rotary precision of the tool is difficult to control (Yan *et al.*, 2010). Ultraprecision broaching is used in the fabrication of complicated spiral cutting paths because of the straight and steep edges of the microlens design, both STS and FTS cannot be used (Li *et al.*, 2012). STS is commonly used for the application with large sag (long Z-axis travel), whereas FTS is used for smoothly changing freeform surfaces (Scheidt *et al.*, 2011). Researchers mostly explore FTS machining for lenslet array due to the flexibility and less cycle time (Yu *et al.*, 2011; Zhu *et al.*, 2017). Compared to FTS, no extra setup is required in STS machining; however, it consumes a lot of time in fabrication due to the lower spindle speeds (Chen *et al.*, 2013; Li *et al.*, 2019; Mukaida *et al.*, 2017). The researchers

show much interest in MLA due to its excellent imaging performance by eliminating aberration and increasing the Field of View (FoV). Yi and Li (Yi *et al.*, 2005) utilized the STS technique for the fabrication of a 5 × 5 MLA on aluminium alloy and demonstrated the possibility of its fabrication. Yu *et al.* (Yu *et al.*, 2012) employed FTS and presented MLAs optimized tool path generation. Mukaida and Yan fabricated a hexagonal microlens array (58 lenslets) on single-crystal silicon in ductile mode by using STS (Mukaida *et al.*, 2017). Kang *et al.* provided an effective method for selection of cutting parameters for concave and convex lenslet arrays by monitoring the position following error for STS (Kang *et al.*, 2022). Tohme (Tohme, 2008) suggested that STS compared to FTS will achieve better surface accuracy without any additional baggage of tool post. Also, the FTS suffers from limited travel distance, which means the peak to valley of the surface it can generate is limited (Tohme *et al.*, 2004). Another limitation is that not every machine has FTS, as it is expensive (Kang *et al.*, 2022). Thus, STS is adopted in this work to fabricate MLA on ZnSe. Subsurface damage, fractures, cracks, and pits are further challenges in the manufacturing of ZnSe. All of these defects will increase light absorption and scattering, having a negative impact on the performance of the optical surface (Ghosh *et al.*, 2018). Also, the path generation and the tool shape compensation need to be taken care of for efficiently producing the contoured shapes with nanometric roughness and submicron form accuracy.

#### 3.1. Tool path generation for microlens array

The traditional SPDT process utilizes two linear axes (X & Z) for contouring the motion, with the spindle controlling the velocity. As a result, this technique can only generate rotationally symmetric surfaces. STS, as an adaptation, allows the spindle to position accurately in a controlled mode. A three-dimensional tool path for the MLA is achieved when the X, Z and C axes move simultaneously according to the specified set of motion commands. In general, the workpiece is positioned on C-axis, while the diamond tool is mounted on the Z-axis, which oscillates forward and backwards in synchronization with the angular position of the C-axis. The control points for STS tool path are laid out in a spiral pattern, and the tool

position is determined by linear interpolation. The control points can be sampled using one of two methods: a) the constant angle technique, and b) the constant arc-length approach. If the control points are separated by constant angle on a spiral tool path it is called as constant angle method, and if the constant arc separates the control points on

a spiral tool path, it is called as constant arc approach. In this study the constant-angle approach is adopted, and the tool path for the current fabrication is generated using DiffSys® (commercial CAM software for ultra-precision turning). The workflow of STS machining of a MLA is illustrated in Fig.3.

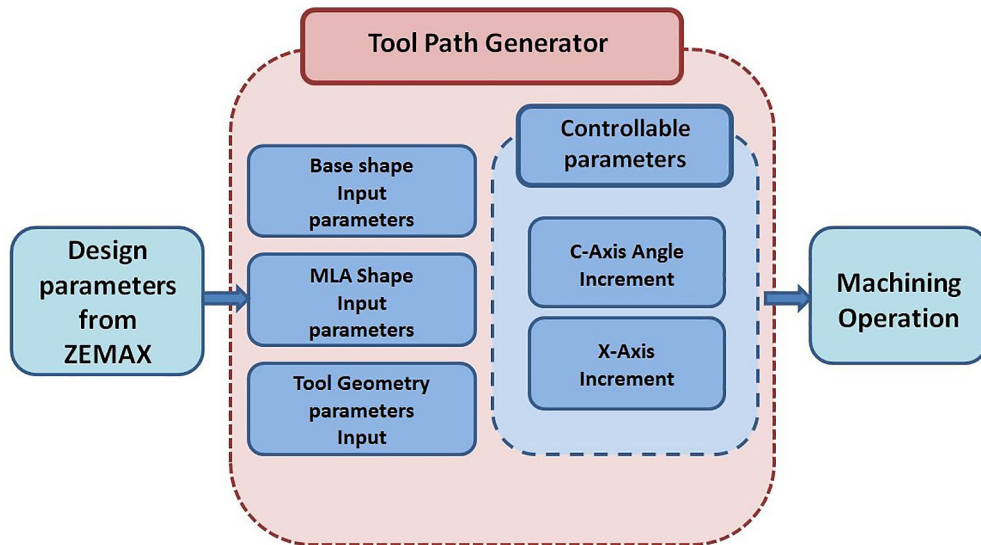


Figure 3. Work Flow for slow tool servo tool path generation.

In STS machining, the coordinate system is described as cylindrical coordinate. The tool path projection on the X-Y plane is equivalent to a spiral curve no matter how complex the surface is (as shown in Fig.4). The spiral curve in the X-Y plane is mathematically represented as follows Eq.4 (Li *et al.*, 2018):

$$\begin{aligned} \rho_i &= R_w - (i-1) \frac{f}{S \cdot N_\theta} \\ \theta_i &= (i-1) \frac{2\pi}{N_\theta} \end{aligned} \quad (4)$$

Where  $i$  ( $i = 1, 2, \dots, \frac{R_w \cdot S \cdot N_\theta}{f} + 1$ ) is number of control points,  $f$  is feed rate in mm/min,  $R_w$  is radius of the workpiece in mm,  $\rho_i$  &  $\theta_i$  are radial distance (cylindrical coordinates) in mm and polar angle (cylindrical coordinates) in radians.  $S$  is spindle speed (rpm),  $N_\theta$  is number of programmed points per revolution.

However, the surface models that need to be fabricated is often expressed in Cartesian coordinate (x,y,z). The translation between the coordinates ( $\rho$  &  $\theta$ ) and (x,y,z) is as Eq.5 (Nagayama *et al.*, 2021).

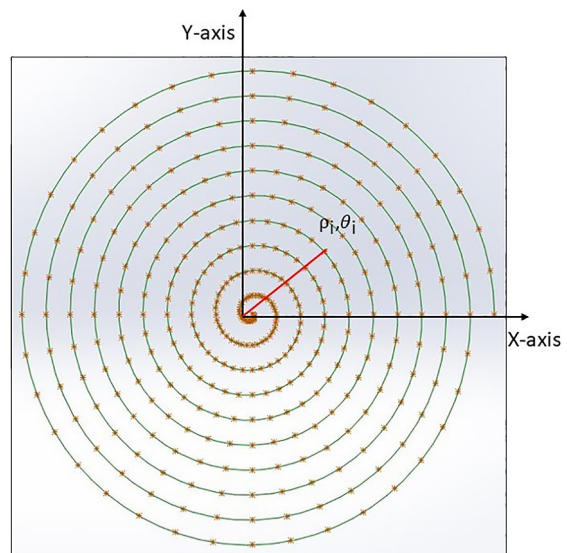


Figure 4. The layout of Control points (Li *et al.*, 2018).

$$\begin{aligned} x &= \rho \cos (\theta) \\ y &= \rho \sin (\theta) \\ z &= f (\rho \cos (\theta), \rho \sin (\theta)) \end{aligned} \quad (5)$$

Where  $f(\cdot)$  describes the designed surface profile, STS ideal tool path for a typical MLA can be generated. It can be mathematically expressed as Eq.6.

$$f(x,y) = A_x \sin\left[\left(\frac{2\pi}{\lambda_x}\right)x + \phi_x\right] + A_y \sin\left[\left(\frac{2\pi}{\lambda_y}\right)y + \phi_y\right] \quad (6)$$

Where  $A_x$  and  $A_y$  are amplitudes,  $\lambda_x$  and  $\lambda_y$  are wavelength and  $\phi_x$  and  $\phi_y$  are phases in x and y directions, respectively.

### 3.2. Experimentation

Using the designed parameters (such as lenslet radius and lenslet pitch as specified in Table.1), the tool path is generated in the form of a polar coordinate system

(CXZ data points) using Diffsys® software. Because of the micro-sized component, a contour makes a diamond tool of zero degrees rake angle with a tool nose radius of 0.2 mm is used for machining. A three-axis SPDT (Precitech make) is used to fabricate MLA as shown in Fig 5. Aluminium fixturing is used to hold and align the ZnSe workpiece. In the case of MLA, spindle speed mainly depends upon these factors: a) the number of X & Z axis travelling within a single rotation of the spindle, b) the magnitude of the sag value when the parametric value of these factors is large, the spindle speed reduces and vice-versa. It is also to be noted that Spindle speed depends on the design data; the controllable parameters are C-axis angle increment and X-axis increment per revolution.

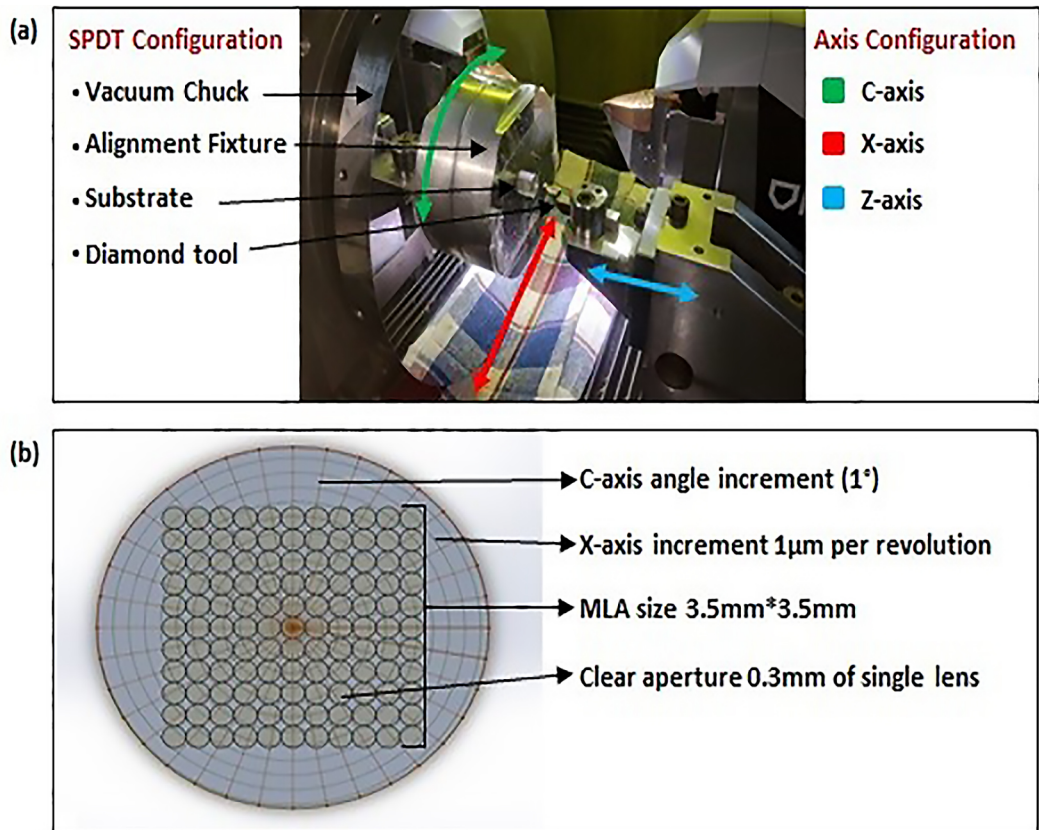


**Figure 5.** Schematic of STS experiment setup (a) C-X-Z configuration, (b) Representative view of controllable parameters.

To achieve optimized cutting speed, the selection of these parameters plays a significant role. Keeping the C-axis angular increment at 1 degree and the X-axis increment per revolution at 1 µm, the machining operation is performed. The total sag value for MLA is 1.238 µm calculated from

design data. During machining, the depth of cut is kept constant at 2 µm keeping all other cutting parameters like tool overhang and mist selection as suggested in the literature (Khatri *et al.*, 2015). A spindle speed of 14 RPM is maintained at the combined feed of the CXZ axis.

#### 4. RESULTS AND DISCUSSION

After fabrication, for characterization, CCI is used with a 5X objective. The CCI images (as shown in Fig.6) of the MLA machined with the optimized parameter indicate that a smooth surface is obtained. All the lenslets shared the same features with no structural and positional distortion, suggesting the MLA was accurately machined. Fig.7 shows the two-dimensional line plots and the form of the machined surface where the value of sag obtained is  $1.206\ \mu\text{m}$ . It can be observed that the total error is  $32\ \text{nm}$  as against the designed value of  $1.238\ \mu\text{m}$ , which is within the tolerance limit. Zhang et al. (Zhang et al., 2020) used a femtosecond laser to fabricate the MLA on ZnSe; results show the root-mean-square deviation between the measured cross-sectional

profile and the ideal parabola was less than  $70\ \text{nm}$ . Guo et al. (Guo et al., 2022) fabricated MLA on isotropic oxygen-free copper using a two-step tool setting method in diamond turning. The surface topography measurement was conducted on a white light interferometer, and an error of  $65\ \text{nm}$  has been obtained. The total error seen in this study is well within the limit, suggesting that the proposed approach achieves high accuracy in one-time cutting, which improves production efficiency. This study clearly shows the feasibility of the STS for the fabrication of ZnSe MLA with desired surface roughness and form accuracies. It should be noted that during the machining of MLA, the form error is possibly due to the tool-related error or a dynamic error. Thus, to further improve the accuracy, there is a need to focus on various error factors and compensation methods.

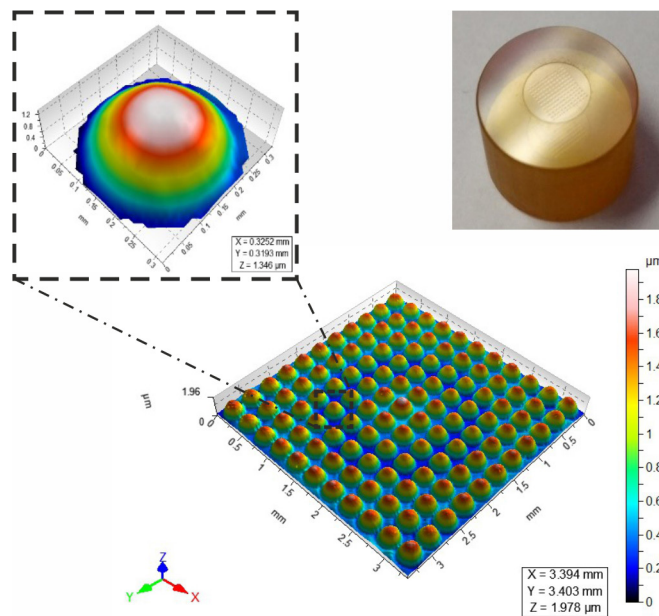


**Figure 6.** Machined lenslet surface CCI measurement.

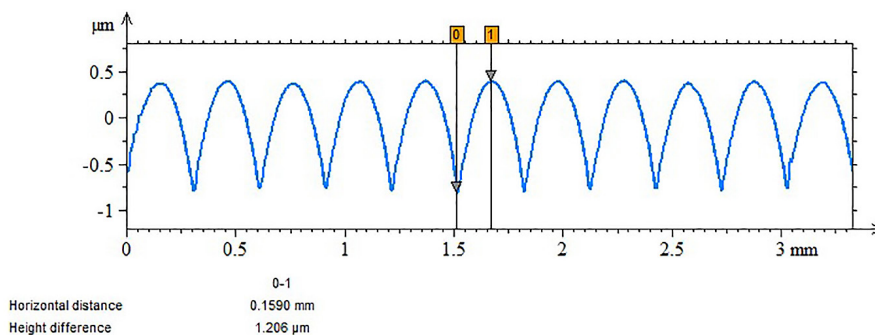


**Figure 7.** 2D plots of the Microlens array.

## 5. CONCLUSION

ZnSe MLAs operating in the mid-IR have attracted more attention for their essential applications in infrared detection, beam homogenization, micro imaging, micro-manufacturing and biochemical systems. In this work, a ZnSe MLA is designed and developed to overcome the depth-of-focus limitation in OCT. Machining of Znse is challenging due to high brittleness, low fracture toughness, and polycrystalline structure formed by the randomly oriented grains. The MLA is fabricated without detectable defects (pits and scratches) on ZnSe material with diamond-turning STS configuration and optimal tool path generation. The experimental validation of the MLA is determined using CCI, and a total error of 32nm is achieved, which is well within the tolerance limit. This research also establishes a substantial base for further developing ZnSe-based lenslet for OCT applications. The proposed MLA has the potential to be an effective tool for confocal imaging, and this advancement will find several applications in the biomedical and other industrial fields. ♦

## REFERENCES

- BERWAL, S., KHATRI, N., & KIM, D. (2022). "A review on design modalities of solar-pumped solid-state laser". *Applied Surface Science Advances*, 12, 100348.
- BO, E., LUO, Y., CHEN, S., LIU, X., WANG, N., GE, X., ... LI, J. (2017). "Depth-of-focus extension in optical coherence tomography via multiple aperture synthesis". *Optica*, 4(7), 701-706.
- CHEN, C.-C., HUANG, C.-Y., PENG, W.-J., CHENG, Y.-C., YU, Z.-R., & HSU, W.-Y. 2013. "Freeform surface machining error compensation method for ultra-precision slow tool servo diamond turning". Paper presented at the Optical Manufacturing and Testing X.
- DING, Z., REN, H., ZHAO, Y., NELSON, J. S., & CHEN, Z. (2002). "High-resolution optical coherence tomography over a large depth range with an axicon lens". *Optics Letters*, 27(4), 243-245.
- DONG, J., GRANT, C., VUONG, B., NISHIOKA, N., GAO, A. H., BEATTY, M., ... GRAHMANN, P. (2022). "Feasibility and safety of tethered capsule endomicroscopy in patients with Barrett's esophagus in a multi-center study". *Clinical Gastroenterology and Hepatology*, 20(4), 756-765. e753.
- GENG, R., YANG, X., XIE, Q., ZHANG, W., KANG, J., LIANG, Y., & LI, R. (2021). "Ultra-precision diamond turning of ZnSe ceramics: Surface integrity and ductile regime machining mechanism". *Infrared Physics & Technology*, 115, 103706.
- GHOSH, G., SIDPARA, A., & BANDYOPADHYAY, P. (2018). "Review of several precision finishing processes for optics manufacturing". *Journal of Micromanufacturing*, 1(2), 170-188.
- GIATTINA, S. D., COURTNEY, B. K., HERZ, P. R., HARMAN, M., SHORTKROFF, S., STAMPER, D. L., ... BREZINSKI, M. E. (2006). "Assessment of coronary plaque collagen with polarization sensitive optical coherence tomography (PS-OCT)". *International Journal of Cardiology*, 107(3), 400-409.
- GUO, P., LI, Z., XIONG, Z., & ZHANG, S. (2022). "A theoretical and experimental investigation into tool setting induced form error in diamond turning of micro-lens array". *The International Journal of Advanced Manufacturing Technology*, 1-11.
- KANG, W., SEIGO, M., XIAO, H., WANG, D., & LIANG, R. (2022). "Experimental Studies on Fabricating Lenslet Array with Slow Tool Servo". *Micromachines*, 13(10), 1564.
- KHATRI, N., SHARMA, R., MISHRA, V., KUMAR, M., KARAR, V., & SAREPAKA, R. V. 2015. "An experimental investigation on the influence of machining parameters on surface finish in diamond turning of silicon optics". Paper presented at the International Conference on Optics and Photonics 2015.
- KLOCKE, F., BRECHER, C., BRINKSMEIER, E., BEHRENS, B., DAMBON, O., RIEMER, O., ... WENZEL, C. (2013). Deterministic polishing of smooth and structured molds. In *Fabrication of complex optical components* (pp. 99-117): Springer.
- LEE, M.-K., & KUO, K.-K. (2007). "Single-step fabrication of Fresnel microlens array on sapphire substrate of flip-chip gallium nitride light emitting diode by focused ion beam". *Applied Physics Letters*, 91(5), 051111.
- LI, D., QIAO, Z., WALTON, K., LIU, Y., XUE, J., WANG, B., & JIANG, X. (2018). "Theoretical and experimental investigation of surface topography generation in slow tool servo ultra-precision machining of freeform surfaces". *Materials*, 11(12), 2566.
- LI, D., WANG, B., QIAO, Z., & JIANG, X. (2019). "Ultra-precision machining of microlens arrays with integrated on-machine surface metrology". *Optics Express*, 27(1), 212-224.

- LI, L., & ALLEN, Y. Y. (2012). "Design and fabrication of a freeform microlens array for a compact large-field-of-view compound-eye camera". *Applied Optics*, 51(12), 1843-1852.
- LIM, C., HONG, M., KUMAR, A. S., RAHMAN, M., & LIU, X. (2006a). "Fabrication of concave micro lens array using laser patterning and isotropic etching". *International Journal of Machine Tools and Manufacture*, 46(5), 552-558.
- LIM, C., HONG, M., LIN, Y., XIE, Q., LUK'YANCHUK, B., SENTHIL KUMAR, A., & RAHMAN, M. (2006b). "Microlens array fabrication by laser interference lithography for super-resolution surface nanopatterning". *Applied Physics Letters*, 89(19), 191125.
- LIU, L., LIU, C., HOWE, W. C., SHEPPARD, C., & CHEN, N. (2007). "Binary-phase spatial filter for real-time swept-source optical coherence microscopy". *Optics Letters*, 32(16), 2375-2377.
- MOORE, S., GOMEZ, J., LEK, D., YOU, B. H., KIM, N., & SONG, I.-H. (2016). "Experimental study of polymer microlens fabrication using partial-filling hot embossing technique". *Microelectronic Engineering*, 162, 57-62.
- MUKAIDA, M., & YAN, J. (2017). "Fabrication of hexagonal microlens arrays on single-crystal silicon using the tool-servo driven segment turning method". *Micromachines*, 8(11), 323.
- NAGAYAMA, K., & YAN, J. (2021). "Deterministic error compensation for slow tool servo-driven diamond turning of freeform surface with nanometric form accuracy". *Journal of Manufacturing Processes*, 64, 45-57.
- NUSSBAUM, P., VOELKEL, R., HERZIG, H. P., EISNER, M., & HASELBECK, S. (1997). "Design, fabrication and testing of microlens arrays for sensors and microsystems". *Pure and applied optics: Journal of the European optical society part A*, 6(6), 617.
- ORTEGA, A., STROJNIK, M., & PAEZ, G. 2007. "Wide-field OCT using micro lens arrays". Paper presented at the Infrared Spaceborne Remote Sensing and Instrumentation XV.
- PODOLEANU, A. G. (2012). "Optical coherence tomography". *Journal of microscopy*, 247(3), 209-219.
- ROMODINA, M. N., & SINGH, K. (2022). "Depth of focus extension in optical coherence tomography using ultrahigh chromatic dispersion of zinc selenide". *Journal of Biophotonics*, e202200051.
- SAKATA, L. M., DELEON-ORTEGA, J., SAKATA, V., & GIRKIN, C. A. (2009). "Optical coherence tomography of the retina and optic nerve – a review". *Clinical & experimental ophthalmology*, 37(1), 90-99.
- SASAKI, K., KUROKAWA, K., MAKITA, S., & YASUNO, Y. (2012). "Extended depth of focus adaptive optics spectral domain optical coherence tomography". *Biomedical Optics Express*, 3(10), 2353-2370.
- SCHEIDING, S., ALLEN, Y. Y., GEBHARDT, A., LI, L., RISSE, S., EBERHARDT, R., & TÜNNERMANN, A. (2011). "Freeform manufacturing of a microoptical lens array on a steep curved substrate by use of a voice coil fast tool servo". *Optics Express*, 19(24), 23938-23951.
- SINGH, K., DION, C., WAJSZILBER, M., OZAKI, T., LESK, M. R., & COSTANTINO, S. (2011). "Measurement of ocular fundus pulsation in healthy subjects using a novel Fourier-domain optical coherence tomography". *Investigative Ophthalmology & Visual Science*, 52(12), 8927-8932.
- SINGH, K., SHARMA, G., & TEARNEY, G. J. (2018). "Estimation and compensation of dispersion for a high-resolution optical coherence tomography system". *Journal of Optics*, 20(2), 025301.
- TOHME, Y. 2008. "Trends in ultra precision machining of freeform optical surfaces". Paper presented at the Optical fabrication and testing.
- TOHME, Y. E., & LOWE, J. A. 2004. "Machining of freeform optical surfaces by slow slide servo method". Paper presented at the Proceedings of the American Society for Precision Engineering (ASPE) Annual Meeting.
- TSAI, T.-H., LEGGETT, C. L., TRINDADE, A. J., SETHI, A., SWAGER, A.-F., JOSHI, V., ... NAMATI, E. (2017). "Optical coherence tomography in gastroenterology: a review and future outlook". *Journal of Biomedical Optics*, 22(12), 121716.
- XIAO, H., LIANG, R., SPIRES, O., WANG, H., WU, H., & ZHANG, Y. (2019). "Evaluation of surface and subsurface damages for diamond turning of ZnSe crystal". *Optics Express*, 27(20), 28364-28382.
- YAN, J., ZHANG, Z., KURIYAGAWA, T., & GONDA, H. (2010). "Fabricating micro-structured surface by using single-crystalline diamond endmill". *The International Journal of Advanced Manufacturing Technology*, 51(9), 957-964.
- YI, A., & LI, L. (2005). "Design and fabrication of a microlens array by use of a slow tool servo". *Optics Letters*, 30(13), 1707-1709.
- YIN, Z., DAI, Y., LI, S., GUAN, C., & TIE, G. (2011). "Fabrication of off-axis aspheric surfaces using a slow tool servo". *International Journal of Machine Tools and Manufacture*, 51(5), 404-410.

- YU, D. P., GAN, S. W., WONG, Y. S., HONG, G. S., RAHMAN, M., & YAO, J. (2012). "Optimized tool path generation for fast tool servo diamond turning of micro-structured surfaces". *The International Journal of Advanced Manufacturing Technology*, 63(9), 1137-1152.
- YU, D. P., WONG, Y. S., & HONG, G. S. (2011). "Optimal selection of machining parameters for fast tool servo diamond turning". *The International Journal of Advanced Manufacturing Technology*, 57(1), 85-99.
- YUAN, W., LI, L.-H., LEE, W.-B., & CHAN, C.-Y. (2018). "Fabrication of microlens array and its application: a review". *Chinese Journal of Mechanical Engineering*, 31(1), 1-9.
- ZHANG, F., YANG, Q., BIAN, H., LIU, F., LI, M., HOU, X., & CHEN, F. (2020). "Fabrication of ZnSe microlens array for a wide infrared spectral region". *IEEE Photonics Technology Letters*, 32(20), 1327-1330.
- ZHU, Z., TO, S., ZHU, W.-L., & HUANG, P. (2017). "Feasibility study of the novel quasi-elliptical tool servo for vibration suppression in the turning of micro-lens arrays". *International Journal of Machine Tools and Manufacture*, 122, 98-105.



**Publisher's note:** Eurasia Academic Publishing Group (EAPG) remains neutral with regard to jurisdictional claims in published maps and institutional affiliations.

**Open Access.** This article is licensed under a Creative Commons Attribution-NonCommercial 4.0 International (CC BY-NC 4.0) licence, which permits copy and redistribute the material in any medium or format for any purpose, even commercially. The licensor cannot revoke these freedoms as long as you follow the licence terms. Under the following terms you must give appropriate credit, provide a link to the license, and indicate if changes were made. You may do so in any reasonable manner, but not in any way that suggests the licensor endorsed you or your use. If you remix, transform, or build upon the material, you may not distribute the modified material. To view a copy of this license, visit <https://creativecommons.org/licenses/by-nc/4.0/>.